Differential vascularization of nematode-induced feeding sites

Stefan Hoth, Ruth Stadler, Norbert Sauer*, and Ulrich Z. Hammes*†

Molecular Plant Physiology, University of Erlangen-Nuremberg, Staudtstrasse 5, 91058 Erlangen, Germany

Edited by Roger N. Beachy, Donald Danforth Plant Science Center, St. Louis, MO, and approved June 16, 2008 (received for review April 23, 2008)

Sedentary nematodes are destructive plant pathogens that cause significant yield losses. In the roots of their host plants, cyst nematodes (CNs) and root-knot nematodes (RKNs) induce different, highly specialized feeding sites—syncytia or giant cells (GCs), respectively—to optimize nutrient uptake. We compared the mechanisms by which nutrients are delivered from the model host plant, Arabidopsis, to GCs induced by the RKN *Meloidogyne incognita* or to syncytia induced by the CN *Heterodera schachtii*. From previous work, syncytia were known to be symplastically connected to newly formed host phloem composed of sieve elements (SEs) and companion cells. Here we studied the formation of plasmodesmata (PD) during GC and syncytia development by monitoring a viral movement protein that targets branched PD and the development of host phloem during GC formation by applying confocal laser scanning microscopy and immunocytochemistry. Analyses of plants expressing soluble or membrane-anchored green fluorescent protein in their phloem demonstrated symplastic isolation of GCs. GCs were found to be embedded in a tissue that consists exclusively of SEs. These *de novo*-formed SEs, contained nuclei and were interconnected by secondary PD. A similar interconnection of SEs was observed around syncytia. However, these secondary PD were also present at the SE–syncytium interface, demonstrating the postulated symplastic connection. Our results show that CNs and RKNs, despite their close phylogenetic relatedness, employ fundamentally different strategies to withdraw nutrients from host plants.

cyst nematode | phloem | plasmodesmata | root-knot nematode

Nematodes are destructive plant pathogens that cause yield losses of billions of US dollars in numerous crop plants (1). Most of the damage is inflicted by sedentary nematodes of the family *Heteroderidae*, which induce specialized feeding sites in infested plant roots, from which nutrients are withdrawn by the parasite. Among this family are cyst nematodes (CNs) and root-knot nematodes (RKNs). In CNs, a syncytium is formed by fusion of neighboring cells (2). In contrast, RKNs form a feeding site by inducing several single cells to become giant cells (GCs) that retain their single-cell identity and undergo marked developmental changes (3). Morphological changes include cell wall ingrowths similar to transfer cells (4). Although both feeding site types go through a different genesis, they yield functionally equivalent structures that act as strong terminal sink tissues (2, 5).

There is an ongoing debate as to how nutrients enter nematode-induced feeding sites from the plant vasculature. In the case of syncytia, microscopy studies as well as microinjection experiments initially suggested the presence of only few plasmodesmata (PD) between syncytia and phloem, which were thought to be non-functional (6, 7). After loading of [^{14}C]-sucrose to source leaves of Arabidopsis, radioactive signals could be monitored along the roots, within syncytia, and in the associated nematodes (8). It was postulated that sucrose transporters are responsible for this accumulation (9, 10). However, despite of the presence of transcripts for these transporters in syncytia, the proteins were not detected (11). On the contrary, it could be demonstrated that soluble green fluorescent protein (sGFP) synthesized in companion cells (CCs) of P_{AtSUC2}:*sGFP* plants (12) entered the syncytia induced by females of *H. schachtii* in roots of these plants. This was not the case when green fluorescent protein (GFP) was fused to a membrane anchor so diffusion of the fluorophore was abolished. This suggested that, despite the predicted low number of non-functional PD, symplastic transport is fundamental for movement of nutrients into syncytia. Furthermore, the induction of CCs and sieve elements (SEs) around syncytia suggested effective nutrient supply by this symplastic pathway (11).

Much less is known about nutrient loading into GCs induced by RKNs, but there is evidence that transmembrane transport processes are more important in this case. Cell wall ingrowths enlarge the surface of GCs as in transfer cells (13), and microarray analyses revealed the induction of 26 genes encoding transport proteins in response to RKN infestation (14), whereas only three such genes are regulated in response to CN infestation (15).

Here we present studies performed on Arabidopsis plants infected with the RKN *Meloidogyne incognita* or the CN *H. schachtii* to address the question how nutrients are delivered to the respective feeding site throughout their development. In case of RKNs, we compared the distribution of sGFP to the localization of membrane-anchored GFP (tmGFP9). These ORFs were expressed under the control of the CC-specific *AtSUC2* promoter (11, 12, 16).

tmGFP9 fluorescence, an indicator of CC identity and thus for the sites of sGFP synthesis, was found exclusively in the vasculature outside the root-knot (RK), but absent from cells surrounding the GCs. In contrast, sGFP showed cell-to-cell movement from the vasculature into a tissue surrounding the GCs, but not into the GCs. These data were corroborated by immunocytochemistry. Localization of the SE-specific RS6 antigen (17) characterized the sGFP-labeled cells surrounding the GCs as SEs. These SEs were formed *de novo* and contained nuclei. The absence of CCs from root-RKs and the presence of CCs in the phloem adjacent to syncytia demonstrated that the vasculature that is formed to supply assimilates to either GCs or syncytia consists of different cell types.

Concomitantly, we monitored the formation of secondary PD during feeding site development in both RKN- and CN-infested plants expressing a fusion construct of GFP to the potato leafroll virus movement protein MP17 (18). Around both syncytia and GCs, the newly formed SEs were heavily interconnected by PD. However, whereas syncytia became connected to the SEs by PD as early as 3 days after infection, GCs remained symplastically

Author contributions: S.H., R.S., N.S., and U.Z.H. designed research; S.H., R.S., and U.Z.H. performed research; S.H., R.S., N.S., and U.Z.H. analyzed data; and N.S. and U.Z.H. wrote the paper.

The authors declare no conflict of interest.

This article is a PNAS Direct Submission.

*To whom correspondence may be addressed. E-mail: ulrich.hammes@biologie.uni-regensburg.de or nsauer@biologie.uni-erlangen.de.

†Present address: Cell Biology and Plant Physiology, University of Regensburg, Universitätsstrasse 31, 93053 Regensburg, Germany.

This article contains supporting information online at www.pnas.org/cgi/content/full/0803835105/DCSupplemental.

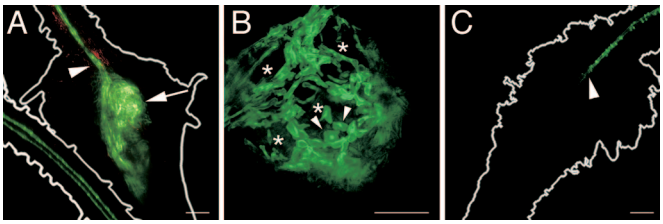

Fig. 1. Fluorescence of sGFP and tmGFP9 in RKs. (*A*) Projection of several confocal sections of sGFP fluorescence in an RK and in an adjacent, uninfected root of a P_{AtSUC2}:*sGFP* plant (18 dai). The outlines of the RK and the uninfested root are shown. GFP fluorescence is seen in the vasculature above the RK (arrowhead) and in cells surrounding the GCs (arrow). As a result of the working distance of the confocal laser scanning microscopy, the vasculature below the RK is not visible. The typical structure of the phloem can be seen in the uninfected root. Red fluorescence results from the autofluorescence of phenolics in the cell wall. (*B*) Single section through a different RK in the same plant line at higher magnification (18 dai). Fluorescence is seen in a net-like structure consisting of small nucleated cells (arrowheads). Fluorescence is absent from large areas inside the RK (asterisks). (*C*) Projection of several confocal sections of tmGFP9 fluorescence in a RK on a P_{AtSUC2}:*tmGFP9* plant (18 dai). The outline of the RK is shown. Fluorescence is restricted to the vasculature above the RK and stops at the position indicated by an arrowhead. As a result of the working distance of the confocal laser scanning microscopy, the vasculature below the RK is not visible. (Scale bars: *A* and *C*, 75 μm; *B*, 150 μm.)

isolated throughout their entire development. Our data suggest that nutrient loading into syncytia occurs symplastically whereas apoplastic loading is fundamental for GCs.

Results

Vascular Disruption and Identification of a Symplastic Domain in RKs. To identify possible changes in vascularization and symplastic continuity in response to RKN infestation, as described for syncytium formation (11), we inoculated P_{AtSUC2}:*sGFP* or P_{AtSUC2}:*tmGFP9* plants (12, 16) with *M. incognita* larvae and screened for GFP fluorescence throughout feeding site development. With respect to feeding sites, both plant lines showed identical distribution of GFP fluorescence in the first 2 weeks of infestation. Fluorescence was restricted to the phloem strands that pass the forming GCs [supporting information (SI) Fig. S1]. After approximately 3 weeks of infestation, when larger GCs had formed and the connectivity of the adjacent root phloem was interrupted, differences between the plant lines became apparent (Fig. 1). In P_{AtSUC2}:*tmGFP9* plants, fluorescence was restricted to the phloem tissue outside the RK (Fig. 1*C*). CCs were no longer detected within the RK (Fig. 1*C*, arrowhead). Fluorescence was never observed within the RK. In P_{AtSUC2}:*sGFP* plants, fluorescence was observed in the phloem outside the RK and in cells surrounding the GCs (Fig. 1*A* and Movie S1). At higher magnification (Fig. 1*B*), fluorescence was observed in a net-like structure consisting of small, nucleate cells (Fig. 1*B*, arrowheads), which surrounded areas that were free of fluorescence (Fig. 1*B*, asterisks). These areas corresponded in shape and size to GCs of that developmental stage.

These findings suggest that, at later stages of GC and feeding site development, CCs within the RK are dissolved or lose their identity, indicated by the termination of *AtSUC2* promoter activity. sGFP, which is synthesized in CCs of the vasculature, can move into a network of cells surrounding the GCs, but not into GCs.

GCs Are Symplastically Isolated. To confirm that the GFP-less areas in the RKs are GCs, RKs of these plants were sectioned to 80 μM on a vibratome. As expected, sGFP fluorescence was restricted to cells surrounding the GCs, but remained absent from the GCs (Fig. 2*A*, asterisks; see Fig. S2 for the transmitted light image).

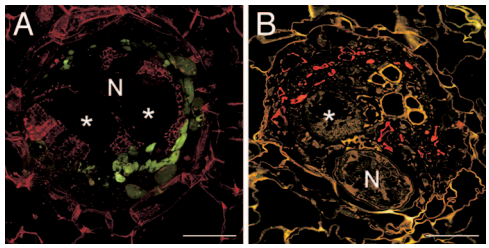

Fig. 2. Localization of sGFP in RKs on P_{AtSUC2}:*sGFP* plants. (*A*) Projection of several confocal sections of GFP fluorescence in an 80-μm vibratome cross section through an RK (18 dai). Fluorescence is seen in small cells within the RK but absent from the GCs (asterisks; N, nematode) (*B*) Immunolocalization of sGFP in a cross section through an RK (18 dai). Anti-GFP-specific fluorescence (red) is limited to cells in the vicinity of GCs but absent from the GCs. sGFP was detected by using a monoclonal anti-GFP antiserum and Cy3-labeled second antibody. (Scale bars, 150 μm.)

To rule out that sGFP fluorescence was not detected in GCs because the fluorophore leaked out of the cells as a result of sectioning of the RKs, we performed immunolocalization of sGFP on fixed and embedded tissue. The results were identical to the ones obtained by direct analysis of sGFP fluorescence: sGFP was detected in cells in direct vicinity of the GCs, but never in the GCs themselves (Fig. 2*B*; see Fig. S2 for the transmitted light image).

Both lines of evidence demonstrate that phloem-derived sGFP moves into a symplastically connected network within the RK, but cannot enter the GCs, suggesting that they are symplastically isolated from the surrounding tissue.

SEs Are Nucleate in RKs. To identify the nature of the tissue type that forms the network surrounding the GCs, we performed immunolocalizations with a monoclonal antibody directed against the SE-specific RS6 antigen (17). The RS6 antibody decorated almost all cells in the direct vicinity of the GCs (Fig. 3*A*). This characterized the GC-surrounding network as SEs, which appear (*i*) to be massively induced in RKs, (*ii*) to be connected to the vascular system of the root phloem, and (*iii*) to form a symplastic domain that allows for macromolecular trafficking.

Typical SEs are terminally differentiated cells and are usually enucleate, and therefore depend on CCs for proper function. However, we did not observe CCs in the RK. Moreover, the subcellular distribution of sGFP in the cells surrounding the GCs (Fig. 1*B*) suggested the presence of nuclei. To test whether the SEs in RKs contain nuclei that enable these SEs to function without CCs, we used the RS6 antibody to label SEs and stained the nuclei with DAPI (Fig. 3*B*). In fact, we could demonstrate DAPI fluorescence inside the RS6-labeled SEs (Fig. 3*B*, arrows, and Fig. S3). This suggested that SEs arising from *de novo* formation in RKs are nucleate and able to function without CCs. To clearly distinguish terminally differentiated, enucleate SEs from the SEs found in RKs, those cells will further be called nucleate SEs (nSEs).

Secondary PD Are Formed Between nSEs. The results obtained by monitoring the movement of sGFP within the RK suggested that PD with a size exclusion limit (SEL) that allows for trafficking of 27-kDa sGFP are present between nSEs. We investigated number and type of PD in RKs on P_{35s}:*MP17-GFP* plants (18). MP17 has been shown to specifically target branched, secondary PD (19). We found that, concomitantly with the formation of the nSE-network and inflow of sGFP into the nSE-network around GCs, a massive induction of PD occurred in RKs (Fig. 3*C*). The pattern observed corresponded to the pattern of sGFP fluorescence seen in Fig. 1*A* (also see Movie S2). A massive induction

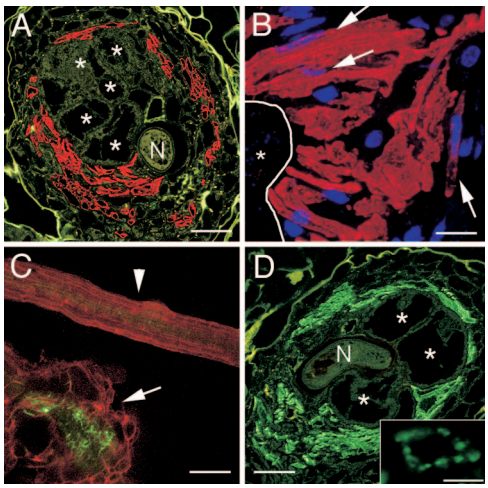

Fig. 3. Localization of PD and SEs in RKs on P_{35S}:*MP17-GFP* plants. (*A*) Cross section through an RK (18 dai). Red fluorescence results from Cy3-labeled second antibody used to detect the SE-specific RS6 antibodies. GCs (asterisks) are embedded in SEs (N, nematode). (*B*) Higher magnification of an area of nSEs directly adjacent to a GC (asterisk). The outline of the GC is indicated by a white line. Red fluorescence results from Cy3-labeled second antibody used to detect the SE-specific RS6 antibodies. Nuclei (blue) are stained with DAPI. Arrows point to nuclei of nSEs. (*C*) Projection of several confocal sections of MP17-GFP fluorescence in an RK (18 dai; arrow) and in an uninfected root (arrowhead). Large numbers of secondary PD are observed within the RK compared with an uninfected root. Red fluorescence results from the autofluorescence of cell wall phenolics. (*D*) Cross section through the same RK as in *A*. MP17-GFP was detected by using a monoclonal anti-GFP antiserum. Green fluorescence results from Cy2-labeled second antibody. Secondary PD are present primarily in the SEs identified in *A* (asterisks; N, nematode). The inlay shows the distribution of PD in the cell wall of one single cell. (Scale bars: *A* and *D*, 150 μm; *B*, 25 μm; *C*, 100 μm; *D inlay*, 5 μm).

of MP17-GFP fluorescence was observed compared with uninfested roots (Fig. 3*C*, arrowhead). This fluorescence was restricted to the direct vicinity of a large area corresponding to the shape and size of GCs, which was free of fluorescence (Fig. S4).

To identify the cells that are interconnected by these secondary PD, we immunolocalized MP17-GFP by using a monoclonal antibody against GFP. The results showed that nSEs, which surrounded GCs, were almost completely perforated by PD in their lateral cell walls (Fig. 3*D*, also see Movie S2).

Taken together, our data show that nSEs are formed *de novo* in direct vicinity of the GCs. These nSEs are not joined by CCs and are heavily interconnected by PD that form a symplastic domain and allow for macromolecular trafficking.

Secondary PD Connect Syncytia to the Phloem. The formation of unloading phloem around syncytia during the infestation with the CN *H. schachtii* has been described (11). In contrast to the situation in RKs, the phloem surrounding syncytia consists of CCs and SEs. Despite the fact that sGFP enters syncytia symplastically, direct evidence of the existence of functional PD connecting syncytia and vasculature was lacking. We investigated whether SEs are connected to syncytia and equally interconnected by PD as the nSEs found in RKs. To this end, we inoculated P_{35S}:*MP17-GFP* plants (18) with *H. schachtii* J2 juveniles and analyzed MP17-GFP localization. CN-induced formation and massive accumulation of secondary PD started 3–5 days after inoculation (Fig. 4 *A* and *B*). At later stages of syncytium formation (14 dai), these PD persisted, were detected mainly in cells surrounding the syncytial structures (Fig. 4*C*), and were found directly at the syncytium interface (Fig. 4*E*). Under the same experimental conditions, secondary PD were hardly found in sections through uninfested roots of a similar age (Fig.

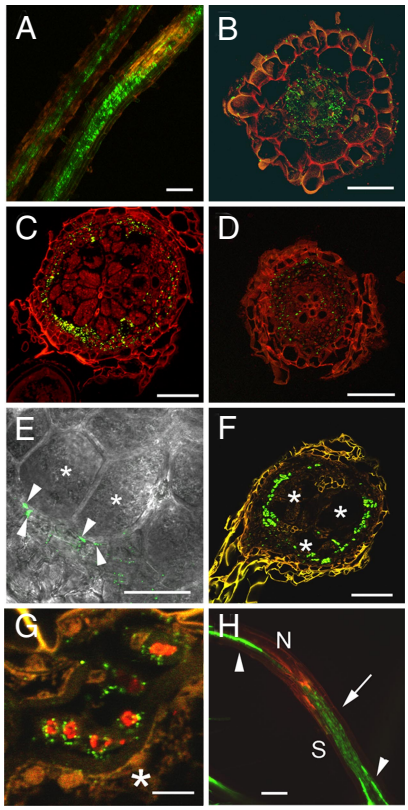

Fig. 4. Formation of PD at syncytia in *H. schachtii*-infected roots. (*A*) Maximum projection of GFP fluorescence in roots of P_{35S}:*MP17-GFP* plants (5 dai). An infected root (*Right*) and an uninfected control root (*Left*) are shown. Induction of PD around syncytial feeding structures is visible. Orange fluorescence is indicative of an infection site. (*B*) MP17-GFP fluorescence in a vibratome cross section of a syncytium (5 dai). Many PD are found in the area of the developing syncytium. (*C*) MP17-GFP fluorescence in a vibratome cross section of a syncytium (14 dai). A large number of PD are arranged at the syncytium surface. (*D*) MP17-GFP fluorescence in a vibratome cross section through an uninfested root displaying regular distribution of only few secondary PD. (*E*) Close-up view of a syncytium (13 dai) with MP17-GFP-labeled PD superimposed onto a transmission light picture. GFP fluorescence indicates the presence of PD at the syncytium–vasculature interface (arrowheads). Syncytial cells are labeled with asterisks. (*F*) Immunolocalization of MP17-GFP protein in a microtome section through a syncytium (14 dai) by monoclonal anti-GFP antibodies. Many PD are seen in the lateral cell walls of cells around the syncytium interface. Syncytial structures are labeled with asterisks. (*G*) Co-immunolocalization of SE-specific RS6 antigen (red) and MP17-GFP fusion protein (green) at the syncytium interface (asterisk). PD are found in the lateral cell walls of SEs that adjoin the syncytium. (*H*) sGFP fluorescence in a syncytium on a P_{AtSUC2}:*sGFP* plant (4 dai). Strong sGFP signals above and below the syncytium are observed in vascular bundles (arrowheads). sGFP fluorescence in the developing syncytium (S, arrow) indicates symplastic loading of sGFP from the phloem into the syncytium. Orange fluorescence is indicative of an infection site (N, nematode). Red fluorescence in *B–D* results from tissue autofluorescence. (Scale bars: *A*, 100 μm; *B*, 40 μm; *C*, *D*, and *F*, 50 μm; *E*, 25 μm; and *G*, 5 μm.)

4*D*). Detection of the MP17-GFP fusion protein with anti-GFP antibodies confirmed that syncytia are surrounded by cells containing high numbers of PD (Fig. 4*F*). To identify the nature of the cells harboring PD, we co-immunolocalized the RS6 antigen and MP17-GFP proteins in microtome sections of syncytia. The same cells were labeled by both fluorescence signals, indicating that the majority of PD is contained in SEs (Fig. 4*G*). In serial sections through syncytia, nuclei could not be detected in these SEs, suggesting that they are typical enucleate SEs. Concomitantly with the formation of secondary PD, macromolecular trafficking of sGFP from these SEs into syncytia via

PD could be observed as early as 3–4 days after inoculation (Fig. 4*H*).

These results suggest that GCs and syncytia are surrounded by high numbers of newly formed SEs that contain a large number of PD. However, whereas a symplastic connection exists between phloem tissue and syncytia, GCs remain very likely symplastically isolated and thus require apoplastic transport for nutrient loading.

Discussion

Symplastic Isolation of GCs. In this study, P_{AtSUC2}:*sGFP* and P_{AtSUC2}:*tmGFP9* plants were used to study possible pathways for nutrient delivery to GCs by mapping symplastic domains and vascular continuity during development of RKs induced by the RKN *M. incognita* in roots of Arabidopsis. The results differed considerably from those obtained for Arabidopsis roots infested with the CN *H. schachtii* (11). In the case of syncytium development, fluorescence of sGFP was found inside the syncytia as early as 3–5 days after infection. This was never observed in GCs throughout the entire development of the RK. Here, fluorescence was found exclusively in numerous nucleated cells embedding the GCs (20). The absence of fluorescence is a result of the absence of the fluorophore, because GFP has been shown to be functional in GCs (20). When *tmGFP9* was expressed from the same promoter, fluorescence remained limited to the phloem outside the RK. Essentially the same result was obtained when the *AtSUC2* promoter was used to drive *GUS* expression (10). This suggests that that CCs are absent from RKs or are degraded or lose their identity, indicated by termination of *AtSUC2* expression, during the process of feeding site formation. In contrast, during syncytium development, CCs were associated with SEs around the syncytia (11). Our data suggest that, in RKs, sGFP, originating from CCs, entered nSEs by mass flow.

nSEs Are Formed *de Novo* in RKs. *De novo* vascularization that supports growth of pathogen-induced tissues with nutrients is a well established phenomenon in animals and plants (21–23). In plants, this response occurs in response to diverse pathogens or parasites (11, 23–25). In all cases of plant–pathogen interaction described so far, the typical structure of the phloem, consisting of SEs and CCs, is maintained. An unloading structure of the phloem in which the ratio of SEs to CCs is shifted in favor of SEs was observed in response to infection of Arabidopsis roots with *H. schachtii* (11). Using the SE-specific RS6 antibody, we were able to show for *M. incognita*-induced RKs that the supply with assimilates is mediated exclusively by cells that possess SE identity and are frequently nucleated, which may be a consequence of their *de novo* formation. These findings are in line with previous reports that suggested expression of the gene encoding the RS6 antigen in young, nucleate SEs and the maintenance of the protein in mature SEs (17).

Role of PD in nSE Symplastic Domain. The CC-less nSE network in RKs forms a hitherto unidentified symplastic domain that serves as a nurse tissue for GCs. The PD interconnecting nSEs display an SEL of at least 27 kDa. As these PD were labeled by MP17, they are of secondary origin. It is long known that SEs contain sieve areas in their lateral cell walls. These sieve areas or pitfields connect SEs among each other. However, they contain simple PD that would not be labeled by MP17 (26). Such pitfields exist in Arabidopsis and can be labeled by other PD proteins (27). To our knowledge, a massive accumulation of secondary PD perforating lateral cell walls to interconnect SEs has not been described.

In contrast to the situation in syncytia (11), we never observed sGFP within the GCs. Nevertheless, it is possible that GCs are connected to the SEs by PD that display a SEL that does not allow for trafficking of sGFP, but would suffice to facilitate symplastic assimilate flow. However, there are a number of arguments that lead us to suggest that GCs are truly symplastically isolated. First, GCs originate from single cells. During their development, they retain their single cell identity, their cell wall thickens considerably, and their surface is further enlarged by cell wall protuberances, which results in a transfer cell-like appearance (13, 28). Generally, transfer cells are found in tissues in which apoplastic transport is fundamental (29). In a study using electron microscopy to monitor the formation of GCs in *Coleus blumei* roots infected with *Meloidogyne arenaria*, transfer cell-like cell wall thickening and protuberances were especially pronounced at the interface between SEs and GCs (13). Finally, no PD were found in a detailed study applying scanning electron microscopy to examine GC cell wall protuberances (30). Second, in a microarray study focusing on the regulation of genes encoding transporters, 26 of these genes were found to be significantly induced upon infection with RKNs, indicating that apoplastic transport plays an important role in providing nutrients to GCs (14). In comparison, only three genes encoding transport proteins were induced upon infestation of Arabidopsis with the beet cyst nematode *H. schachtii* (15).

In contrast to the concept of apoplastic loading proposed here, one study found that the phloem mobile tracer carboxyfluorescin (CF) accumulated in GCs when this dye was applied to leaves of tomato (31). The authors concluded that CF was transported in the phloem and entered GCs via symplastic connections. However, CF fluorescence was found in GCs 2 days after its application to leaves. When applied to leaves of Arabidopsis, CF fluorescence occurred rapidly after a couple of minutes in roots (32). Correspondingly, following application of CF to tomato leaves, CF fluorescence should appear in roots at 1–2 hours if the dye is transported via the phloem and symplastically released into the GCs. The very long time of 2 days is sufficient to allow CF diffusion to the RK in the apoplast (33). Even though CF is relatively membrane-impermeant, incorporation of this dye across membranes does take place at slow rates (33, 34). The observed accumulation of CF in GCs can alternatively be explained by the enhanced incorporation associated with the huge surface of these cells.

Phloem Unloading in RKs. Obviously, our data raise an important question: how is unloading of assimilates from nSEs into the apoplast facilitated? There are two possible explanations that may work in combination. The first is active nursing of the GC apoplast by the nSEs. This implicates that nSEs found adjacent to GCs assume a function similar to tapetum cells. In this case, nutrients would be loaded into the apoplast by means of hitherto unidentified export proteins or by exocytosis. The second is passive diffusion from the phloem into the apoplast, which is believed to mediate the transition from symplastic to apoplastic nutrient flow into lateral and terminal sink tissues (35, 36). The massive induction of nSEs is increasing the surface for nutrient unloading into the apoplast. The direction of assimilate flow from the apoplast is dependent on the chemical gradient, which, because of the high sink strength, is directed toward GCs. Additionally, because of the lack of CCs, the sucrose transporters AtSUC2 and AtSUC3, which have been postulated to retrieve sucrose that is lost from the phloem along the transport pathway, are absent from RKs (37, 38). Consequently, nSEs lack the ability to retrieve sucrose. Subsequently, import of assimilates into GCs is facilitated by sink tissue-localized transporters that have been implicated in GC nutrition (14, 39).

Regardless of the actual unloading mechanism, it appears that GCs, in contrast to syncytia, are loaded by an apoplastic pathway.

Nutrient Loading into Syncytia Occurs via PD. A huge body of work exists on the ultrastructure of GCs and syncytia. As a result of

the greater agronomic impact of CNs, more focus has been put on syncytia. However, molecular approaches using marker lines to identify tissues and genes involved in nutrient loading are still fairly limited. For a long time it has been postulated that syncytia induced by *H. schachtii* are symplastically isolated, because only few PD, which appeared to be modified, were observed (8, 10, 24, 40). In contrast, PD were found in syncytia induced by the false RKN *Nacobbus aberreans* in tomato roots, and a role for PD in nutrition was suggested (41). It was not until recently that diffusion of sGFP from the phloem into syncytia induced by *H. schachtii* directly implicated a symplastic connection between these tissues (11). In the present study, we provide direct evidence of the existence of functional PD connecting SEs among each other and to the syncytium (Fig. 4*G*). A significant increase in PD frequency occurred as early as 3 days, simultaneous to the occurrence of sGFP fluorescence.

In contrast to the symplastic loading concept, it has been suggested that the sucrose transporters AtSUC2 and AtSUC4 are crucial for importing sucrose into syncytia, especially during the first days of infection, when symplastic pathways might not yet be functional (9). In fact, mRNA for both transporters was found in syncytia. However, given the fact that syncytia are symplastically connected to the phloem, it is well possible that any RNA in the phloem sap might also be present in syncytia (for a recent review, see ref. 42). There are several additional objections to a role for these transporters in loading sucrose into syncytia. First, expression of AtSUC2 is even decreased in the early days of syncytium development (9). A role for this transporter at later stages of syncytium development is unlikely as it has been clearly demonstrated that the AtSUC2 protein is absent from syncytia (11). Second, a role for AtSUC4 in apoplastic loading of sucrose into syncytia is unlikely, because this protein is localized to the tonoplast (43). The observation that fewer females were found on roots of Arabidopsis plants in which the *AtSUC4* gene was silenced (9) raises the interesting question how subcellular compartmentation of carbohydrates influences nematode development.

To date there is no evidence for the elevated accumulation of transport proteins in syncytial membranes. The occurrence of PD at very early stages of infection rather suggests that symplastic loading is sufficient to support nutrient supply of the feeding site.

Conclusion

RKN and CN belong to the same family of nematodes. Despite their close phylogenetic relatedness, the feeding sites induced by these two types of nematodes use fundamentally different strategies for nutrient import. In the case of RKN-induced GCs, assimilate loading occurs apoplastically by transport proteins, whereas CN-induced syncytia are loaded symplastically via PD. These different strategies may explain why the host range of RKNs is wider than that of CNs and adds further support to the idea of convergent evolution of CNs and RKNs, suggesting that these two genera are much more diverged than previously expected (44). The apoplastic loading of nutrients into GCs implies that transport proteins may prove to be useful targets for RKN control by transgenic or pharmacological approaches. Additionally, nematode-induced feeding sites may provide a useful tool to study vascularization of pathogen-induced tissues as well as early events of phloem development.

Methods

Strains. Transgenic Arabidopsis lines, in which the *AtSUC2* promoter is used to drive expression of the ORFs for sGFP [P_{AtSUC2}*:sGFP* (12)] or tmGFP9 [P_{AtSUC2}*:tmGFP9* (16)] or expressing potato leafroll virus movement protein MP17 fused to GFP under control of the constitutive cauliflower mosaic virus *35S* promoter [P_{35S}*:MP17-GFP* (18)], were infected with the beet CN *H. schachtii* or the RKN *M. incognita*.

Growth Conditions and Infection with Nematodes. Seeds of the lines described earlier were surface sterilized in 1.5% sodium hypochlorite and 0.05% Tween 20 for 5 min and washed three times with sterile water. Sterilized seeds were resuspended in 0.1% agarose and sown on Petri dishes containing Murashige and Skoog medium (pH 5.7, 1% sucrose, 0.8% phytoagar).

Plant growth and infection with *H. schachtii* was performed as described (11). In case of *M. incognita,* plant growth and infection were performed as described (14) with the following modification: plants were inoculated with freshly hatched J2 juveniles from surface sterilized eggs (45).

Section Preparation and Immunohistochemistry. For vibratome sectioning (Model 1500; The Vibratome Company), RKs and syncytia were treated as described (39) without fixation. For immunohistochemistry, roots with syncytia or RKs were embedded in methacrylate sectioned into 3-μm slices (Ultracut R; Leica Microsystems) and treated with antibodies as described (46). Antibodies were diluted in blocking buffer as follows: monoclonal mouse RS6 antibody 1:5 (17, 38); polyclonal rabbit anti-GFP antiserum 1:100 (Invitrogen); monoclonal mouse anti-GFP antiserum 1:200 (Millipore); and anti-rabbit IgG-Cy2 conjugate, anti-mouse-Cy2 and Cy3 conjugates 1:50 (Dianova). For DAPI staining, antibody-decorated sections were mounted in 50 mM Tris·HCl, pH 7.5, 150 mM NaCl, 50% glycerol, 0.2 μg/ml DAPI (Roth).

Confocal Laser Scanning Microscopy. High-resolution images of GFP fluorescence and immunohistochemical analyses were made with a confocal laser scanning microscope (TCS SP II; Leica Microsystems) as described (11, 16). Confocal images were processed using Leica Confocal Software 2. GFP as well as Cy2 were excited with an argon laser at 488 nm, and fluorescence was recorded in a window ranging from 595 to 640 nm. Cy3 was excited with an argon laser at 543 nm, and fluorescence was recorded in a window ranging from 552 to 617 nm. DAPI was excited using the 405-nm diode, and fluorescence was recorded in a window ranging from 417 to 474 nm.

ACKNOWLEDGMENTS. We thank Prof. Uwe Sonnewald for making the P_{35S}*:MP17-GFP* plants available and Gary Thompson for providing the RS6 antiserum; Leo Altena and Jan van de Haar (HZPC research, Metslawier, The Netherlands) for supplying nematodes; and Helen Fuchs for critical comments on the manuscript. This work was funded by DFG grants HA 3468/2-1 and HA 3468/3-1 (to U.Z.H.) and by the Körber European Science Award (to N.S.).

1. Sasser JN, Freckman DW (1987) in *Vistas in Nematology*, eds Dickson DW, Veech J (Soc. Nematologists Inc., Hyattsville, MD), pp 7–14.
2. Jones MGK, Northcote DH (1972) Nematode-induced syncytium - a multinucleate transfer cell. *J Cell Sci* 10:789–809.
3. Bird DM (2004) Signaling between nematodes and plants. *Curr Opin Plant Biol* 7:372–376.
4. Jones MGK, Payne HL (1978) Early stages of nematode-induced giant-cell formation in roots of. *Impatiens balsamina*. *J Nematol* 10:70–84.
5. McClure MA (1977) Meloidogyne incognita: a metabolic sink. *J Nematol* 9:88–90.
6. Grundler FMW, Sobczak M, Golinowski W (1998) Formation of cell wall openings in root cells of *Arabidopsis thaliana* following infection by the plant-parasitic nematode *Heterodera schachtii*. *Eur J Plant Pathol* 104:545–551.
7. Böckenhoff A, Grundler FMW (1994) Studies on the nutrient uptake by the beet cyst nematode *Heterodera schachtii* by in situ microinjection of fluorescent probes into the feeding structures in *Arabidopsis thaliana*. *Parasitology* 109:249–255.
8. Böckenhoff A, Prior DA, Grundler FMW, Oparka KJ (1996) Induction of phloem unloading in *Arabidopsis thaliana* roots by the parasitic nematode *Heterodera schachtii*. *Plant Physiol* 112:1421–1427.
9. Hofmann J, Wieczorek K, Blochl A, Grundler FM (2007) Sucrose supply to nematode-induced syncytia depends on the apoplasmic and symplasmic pathways. *J Exp Bot* 58:1591–1601.
10. Jürgensen K, *et al.* (2003) The companion cell-specific Arabidopsis disaccharide carrier AtSUC2 is expressed in nematode-induced syncytia. *Plant Physiol* 131:61–69.
11. Hoth S, *et al.* (2005) Nematode infection triggers the de novo formation of unloading phloem that allows macromolecular trafficking of green fluorescent protein into syncytia. *Plant Physiol* 138:383–392.
12. Imlau A, Truernit E, Sauer N (1999) Cell-to-cell and long-distance trafficking of the green fluorescent protein in the phloem and symplastic unloading of the protein into sink tissues. *Plant Cell* 11:309–322.
13. Jones MGK, Northcote DH (1972) Multinucleate Transfer Cells Induced in Coleus Roots by the Root-Knot Nematode, *Meloidogyne arenaria*. *Protoplasma* 75:381–395.
14. Hammes UZ, *et al.* (2005) Nematode-induced changes of transporter gene expression in Arabidopsis roots. *Mol Plant Microbe Interact* 18:1247–1257.
15. Puthoff DP, Nettleton D, Rodermel SR, Baum TJ (2003) Arabidopsis gene expression changes during cyst nematode parasitism revealed by statistical analyses of microarray expression profiles. *Plant J* 33:911–921.

16. Stadler R, *et al.* (2005) Expression of GFP-fusions in Arabidopsis companion cells reveals non-specific protein trafficking into sieve elements and identifies a novel post-phloem domain in roots. *Plant J* 41:319–331.
17. Khan JA, *et al.* (2007) An early nodulin-like protein accumulates in the sieve element plasma membrane of Arabidopsis. *Plant Physiol* 143:1576–1589.
18. Vogel F, Hofius D, Sonnewald U (2007) Intracellular trafficking of Potato leafroll virus movement protein in transgenic Arabidopsis. *Traffic* 8:1205–1214.
19. Hofius D, *et al.* (2001) Evidence for expression level-dependent modulation of carbohydrate status and viral resistance by the potato leafroll virus movement protein in transgenic tobacco plants. *Plant J* 28:529–543.
20. Urwin PE, *et al.* (1997) Continual green-fluorescent protein monitoring of cauliflower mosaic virus 35s promoter activity in nematode-induced feeding cells in Arabidopsis thaliana. *Mol Plant Microbe Interact* 10:394–400.
21. Folkman J (1985) Tumor angiogenesis. *Adv Cancer Res* 43:175–203.
22. Ullrich CI, Aloni R (2000) Vascularization is a general requirement for growth of plant and animal tumours. *J Exp Bot* 51:1951–1960.
23. Wächter R, *et al.* (2003) Vascularization, high-volume solution flow, and localized roles for enzymes of sucrose metabolism during tumorigenesis by *Agrobacterium tumefaciens*. *Plant Physiol* 133:1024–1037.
24. Golinowski W, Grundler FMW, Sobczak M (1996) Changes in the structure of *Arabidopsis thaliana* during female development of the plant-parasitic nematode *Heterodera schachtii*. *Protoplasma* 194:103–116.
25. Haupt S, Oparka KJ, Sauer N, Neumann S (2001) Macromolecular trafficking between *Nicotiana tabacum* and the holoparasite *Cuscuta reflexa*. *J Exp Bot* 52:173–177.
26. Behnke H-D, Schulz A (1980) Fine structure, pattern of division, and course of wound phloem in *Coleus blumei*. *Planta (Berl)* 150:357–365.
27. Thomas CL, *et al.* (2008) Specific targeting of a plasmodesmal protein affecting cell-to-cell communication. *PLoS Biol* 6:e7.
28. Bird AF (1961) The ultrastructure and histochemistry of a nematode-induced giant cell. *J Biophys Biochem Cytol* 11:701–715.
29. Offler CE, McCurdy DW, Patrick JW, Talbot MJ (2003) Transfer cells: Cells specialized for a special purpose. *Annu Rev Plant Biol* 54:431–454.
30. Jones MG, Dropkin VH (1976) Scanning electron microscopy in nematode-induced giant transfer cells. *Cytobios* 15:149–161.
31. Dorhout R, Gommers FJ, Kollöffel C (1993) Phloem transport of carboxyfluorescin through tomato roots infected with *Meloidogyne incognita*. *Physiol Mol Plant Pathol* 43:1–10.
32. Oparka KJ, Duckett CM, Prior DAM, Fischer DB (1994) Real-time imaging of phloem unloading in the root tip of Arabidopsis. *Plant J* 6:759–766.
33. Kramer EM, Frazer NL, Baskin TI (2007) Measurement of diffusion within the cell wall in living roots of *Arabidopsis thaliana*. *J Exp Bot* 58:3005–3015.
34. Wright KM, Horobin RW, Oparka KJ (1996) Phloem mobility of fluorescent xenobiotics in Arabidopsis in relation to their physicochemical properties. *J Exp Bot* 47:1779–1787.
35. Hafke JB, *et al.* (2005) Thermodynamic battle for photosynthate acquisition between sieve tubes and adjoining parenchyma in transport phloem. *Plant Physiol* 138:1527–1537.
36. Patrick JW (1997) Phloem unloading: Sieve element unloading and post-sieve element transport. *Annu Rev Plant Physiol Plant Mol Biol* 48:191–222.
37. Martens HJ, Roberts AG, Oparka KJ, Schulz A (2006) Quantification of plasmodesmatal endoplasmic reticulum coupling between sieve elements and companion cells using fluorescence redistribution after photobleaching. *Plant Physiol* 142:471–480.
38. Meyer S, *et al.* (2004) Wounding enhances expression of AtSUC3, a sucrose transporter from Arabidopsis sieve elements and sink tissues. *Plant Physiol* 134:684–693.
39. Hammes UZ, *et al.* (2006) AtCAT6, a sink-tissue-localized transporter for essential amino acids in Arabidopsis. *Plant J* 48:414–426.
40. Jones MGK (1981) in *Plant Parasitic Nematodes*, eds Zuckerman BM, Rohde RA (Academic, New York), Vol 3, pp 255–279.
41. Jones MGK, Payne HL (1977) The structure of syncytia induced by the phytoparasitic nematode *Nacobbus aberreans* in tomato roots, and the possible role of plasmodesmata in their nutrition. *J Cell Sci* 23:299–313.
42. Kehr J, Buhtz A (2008) Long distance transport and movement of RNA through the phloem. *J Exp Bot* 59:85–92.
43. Endler A, *et al.* (2006) Identification of a vacuolar sucrose transporter in barley and Arabidopsis mesophyll cells by a tonoplast proteomic approach. *Plant Physiol* 141:196–207.
44. Scholl EH, Bird DM (2005) Resolving tylenchid evolutionary relationships through multiple gene analysis derived from EST data. *Mol Phylogenet Evol* 36:536–545.
45. Hussey RS (1985) in *An Advanced Treatise on Meloidogyne*, eds Sasser JN, Carter CC (North Carolina State University Graphics, Raleigh, NC), Vol 1, pp 143–153.
46. Stadler R, Sauer N (1996) The *Arabidopsis thaliana AtSUC2* gene is specifically expressed in companion cells. *Botanica Acta* 109:299–306.